

# Rugate filters for OH-suppressed imaging at near-infrared wavelengths

Alison R. Offer<sup>1</sup> and Joss Bland-Hawthorn<sup>2</sup>

<sup>1</sup>Anglo-Australian Telescope, Siding Spring Observatory, Coonabarabran, NSW 2357, Australia

<sup>2</sup>Anglo-Australian Observatory, P.O. Box 296, Epping, NSW 2121, Australia

9 September 2018

## ABSTRACT

Ground based observations at near-infrared wavelengths are severely affected by atmospheric OH bands. Many authors have recognized the potential gains in sensitivity from suppressing these features. Dispersive instruments show some promise but are both expensive and complicated to build. OH suppression filters using single (Herbst 1994) or periodic notches (Jones et al. 1997) have the advantage of simplicity but significant gains have not yet been realised.

Rugate filters (with graded index inhomogeneous coatings) offer key advantages for astronomical imaging. It is possible to produce a transmission profile comprising a series of irregular and sharply defined bandpasses. We demonstrate through numerical simulation of rugate filters that it should be possible to achieve 95% suppression of the OH features in the *J* photometric band, while retaining roughly half of the spectral coverage. This would lead to extraordinary gains in sensitivity even for observations of continuum sources. In addition, these filters allow longer exposures before the detector saturates on the sky background. *I* and *z*-band filters can also be envisaged.

In 1'' seeing, a *J*-band rugate filter used in conjunction with a 4m telescope would detect a  $J = 23$  continuum source at  $5.0\sigma$  in a single 10 min exposure. In comparison, a conventional *J* filter requires multiple exposures for a 10 minute integration time and achieves only a  $2.5\sigma$  detection. For emission line sources, the rugate filter has an even bigger advantage over conventional filters, with a fourfold increase in signal:noise ratio possible in certain instances.

Astrophysical studies which could benefit from rugate filters are searches for very low mass stars and galaxy evolution out to  $z = 3$ .

## 1 INTRODUCTION

The night sky spectrum in the near infrared is dominated by bright emission lines from vibrationally and rotationally excited OH molecules in the mesosphere and lower thermosphere (80-100km altitude). The principle source of the OH molecules is believed to be the reaction between atomic hydrogen and ozone (Bates & Nicolet 1950) which produces OH in vibrational states up to  $\nu = 9$ . The subsequent decay of the excited OH, along with a small contribution from other processes, is believed to be responsible for the OH emission (Bates 1982; Le Texier et al. 1987). The OH emission can vary both temporally and spatially across the sky (Johnston & Broadfoot 1993; Ramsay et al. 1992). In particular, the propagation of density and temperature differences through the atmosphere can cause large variations in both the relative and absolute intensity of the OH lines with periods as short as a few minutes. The presence of this intense and variable background is a serious problem for earth-based astronomical observations in the near infra-red. In the *J* photometric band (1.12 $\mu$ m to 1.38 $\mu$ m) around 95% of the sky background is in the form of line emission, principally OH. The OH emission in the *I* photometric band is less

intense but is still a large percentage of the background. Clearly there would be large potential gains if the OH emission could be suppressed, both in terms of the improvement in signal to noise ratio if the sky background were reduced by over 90%, and in terms of the increased exposure time a much reduced and more stable sky background would allow.

There has been an increasing interest in methods of suppressing the OH background. These can be grouped into dispersive solutions (Maihara 1994; Iwamuro et al. 1994; Content & Angel 1994; Content 1996; Piché et al. 1997) and filter based solutions (Jones et al. 1997). Filter based solutions have the advantage of being relatively simple, especially for imaging purposes. However, numerical simulations of filter based solutions have been generally disappointing (Herbst 1994; Jones et al. 1997) and attention has been directed towards dispersive solutions. Filter based solutions have suffered from the inflexibility of simple filter profiles. Herbst (1994) investigated bandpass filters but found only a moderate improvement in the sensitivity for the *J* band. Jones et al. (1997) investigated the use of multiple bandpass filters but the improvement in sensitivity was limited by problems matching the periodic transmittance profile to

the OH emission. However, recent advances in filter technology, driven by the development of highly wavelength specific laser rejection filters (Johnson & Crane 1993), mean that filters with almost any transmittance profile can be designed and tailored to a particular problem. It is therefore possible to design of an on-off filter with pass bands at any desired wavelength. A filter blocking most of the OH lines individually is infeasible but there are no technical limitations to building an on-off filter which masks regions of the spectrum overwhelmed by bright OH vibrational bands, whilst retaining roughly half the spectral coverage. Such rugate devices can now be manufactured and promise major gains for wide-field imaging.

In this paper, it is demonstrated that significant gains in the broad-band signal to noise ratio can be envisaged using the ideas of rugate filter design. By exploiting the fact that the intense OH lines at wavelengths of less than  $1.4\mu\text{m}$  are grouped into distinct and non-overlapping bands, large increases in the signal to noise ratio can be achieved in the  $J$  photometric band. The gains in the  $I$  photometric band depend on the assumed background continuum level, but worthwhile increases in the signal to noise ratio can be found if the continuum is small. The first section of the paper introduces the rugate filter concept. A basic design strategy is outlined in section 2 and section 3 describes the signal to noise ratio calculations. The results are presented in section 4. Section 5 discusses the practicality of manufacturing such filters and a brief discussion on how the concepts used could be extended and applied to other problems. The paper concludes with a summary in section 6.

## 2 RUGATE FILTERS

Rugate\* filters are thin film filters with refractive indices that vary continually through the thin film coating (Johnson & Crane 1993). They are manufactured by carefully controlling the chemical composition of a mixture of thin film materials with different individual refractive indices during deposition. In the simplest case, a rugate filter with an infinitely long sinusoidal refractive index profile gives a transmittance profile with a single minimum at a wavelength of  $\lambda = 2n_a x_P$  where  $n_a$  is the average refractive index and  $x_P$  is the geometric period. The width of the minimum is related to the amplitude of the sinusoid (a narrow minimum corresponds to a small amplitude). For a given period and amplitude, the sharpness of the transmittance profile is related to the number of periods included in the filter (a longer filter gives a sharper transmittance minimum). A superposition of two sinusoids gives two transmittance minima with positions dependent on the individual periods and widths dependent on the individual amplitudes.

The relationship between a sinusoidal filter and a quarter wave stack can be understood by analogy with Fourier theory. A quarter wave stack has a square refractive index profile, and therefore requires an infinite number of sinusoids to represent it, with the fundamental geometric period being  $P = \lambda/2n_a$ . The quarter wave stack thus gives transmittance minima at  $\lambda = 2n_a x_P/m$  ( $m = 1, 2, 3, \dots$ ).

\* The name derives from the Latin word for ‘wrinkled’ which describes the refractive index structure.

Between the two limits there is an infinite range of possible filter profiles. In principle filters giving complex and sharply varying transmittance curves can be designed by tailoring the refractive index profiles. Apodisation of the profiles, and quintic matching layers at the air/rugate and rugate/substrate interfaces can be used to reduce reflection losses and sidelobes in the transmission profiles of real filters with a finite extent (Southwell 1989; Southwell & Hall 1989; Fabricius 1992).

The possibility of being able to design filters with a small number of transmittance minima at any chosen wavelength and for any desired width has not previously been considered when considering filter based solutions to the OH suppression problem.

## 3 FILTER DESIGN

The design of a filter with a given transmittance profile is a typical example of an inverse problem. Although the relationship between the transmission profile and refractive index profile can be understood by analogy to Fourier theory, no exact transformation between the two exists. The forward problem – given a refractive index profile, find its transmittance profile – is straight forward, but the inverse of this is, in general, non-trivial and the solution is non-unique. There is a wide range of literature dealing with solutions to the inverse problem using either methods based on Fourier transforms or optimisation techniques, or a combination of the two (Dobrowolski & Verly 1993). The details and relative merits of the methods are beyond the scope of this paper. To illustrate the idea of using rugate filters for OH suppression we only require a basic method to optimise a profile. The aim here is not to design a perfect filter but to illustrate that realistic transmission profiles can be produced that significantly reduce the OH background in the near infra-red. To this end, it was assumed that the refractive index profile could be written as the sum of a small number of sinusoids and the parameters were optimised using a genetic algorithm (GA) approach (Goldberg 1989). The use of Genetic Algorithms to design multilayer filters has been discussed by Martin et al. (1995) and Greiner (1996). Martin et al. and Greiner both use GA to optimise the thicknesses and refractive indices of the individual layers in multilayer stacks. The implementation of GA used here was slightly different. The GA sought to optimise the amplitude, phase and period of a sum of sinusoids representing the refractive index profile. The algorithm used was based on the method outlined by Charbonneau (1995). It is described in more detail in the appendix but in outline it entails constructing an initial random population of solutions. The members of the population are ranked according to their fitness (or the extent to which they minimise or maximise some function). The population is then allowed to evolve towards an optimal solution through a series of breeding and mutation operations. This approach had the advantage of allowing the possibility of simultaneous optimisation of the refractive indices through the filter and the transmission profile itself. It was therefore possible to seek directly the transmission profile that gave the optimum improvement in sensitivity.

The sky spectrum in the  $I$ ,  $J$  and  $H$  bands is shown in figure 1. The emission lines are principally OH although

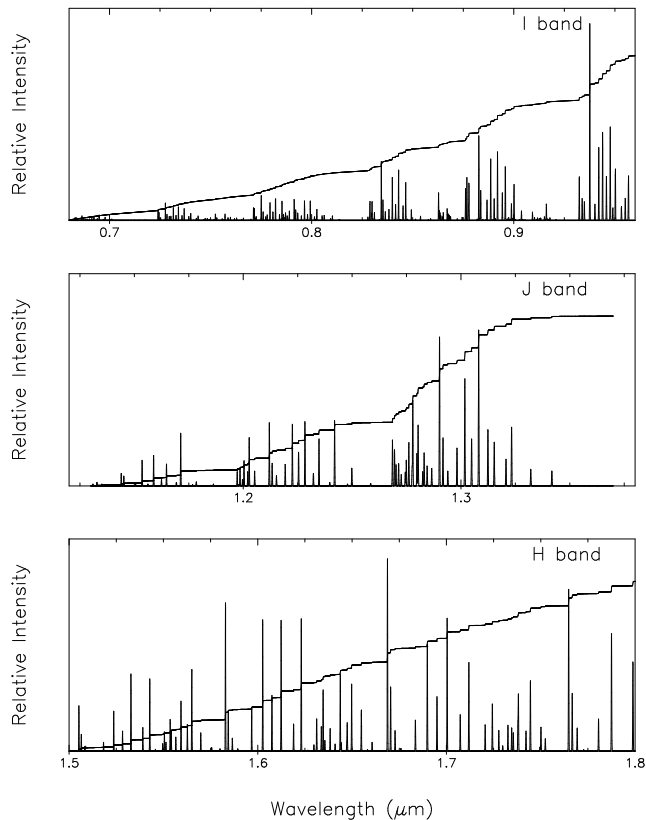


**Figure 1.** The sky spectrum in the *I*, *J* and *H* bands. Note that the *J* band OH lines are grouped into a series of non-overlapping vibrational bands. In the *I* band there is some overlap but the most intense OH emission is concentrated in a few spectral regions. In the *H* band the vibrational bands overlap and the OH lines are more evenly distributed. The continuous line is the cumulative background intensity as a function of wavelength through the band.

there are oxygen bands around  $1.27\mu\text{m}$  and  $0.865\mu\text{m}$ . Also shown is the cumulative background intensity as a function of wavelength. In the *I* and *J* bands the OH lines are grouped into a few main bands separated by relatively clean windows and the cumulative background intensity has a step-like profile. This suggests the approach of seeking a *I* and *J* filters that give a transmittance close to unity in the windows and close to zero around the OH bands. An alternative approach would be to attempt to block individual OH lines. The latter approach is the method adopted by most dispersive OH suppression methods. It could potentially give a greater improvement in the signal to noise ratio for continuum objects because more object flux would be retained. However, because of the intrinsic width of filter profiles, this is infeasible for filter based solutions and the first approach was adopted. Note that in the *H* band the OH vibrational bands overlap and the cumulative intensity has a smoother gradient. Effective OH suppression would require a far more complicated transmission profile so consideration was limited to the *I* and *J* bands.

In outline, the basis approach used for this illustration was as follows:

- (i) Seek for an ‘ideal’ filter profile with a few blocking

bands optimally positioned for maximum signal:noise improvement

- (ii) Use the ‘ideal’ filter as an initial goal for a genetic algorithm seeking to optimise a small number of sinusoids. This produces an approximation to a relatively simple square wave profile.

- (iii) As the ‘ideal’ transmittance profile is approached, optionally switch to a genetic algorithm seeking to maximise a function of the percentage of object flux retained and the increase in the signal:noise ratio. This step improves the theoretical performance of the filter at the expense of producing more complex (therefore less robust) transmission profiles.

To select an ‘ideal’ filter, it was assumed that the maximum signal:noise gain would be achieved when the boundaries of the block were set just outside two OH lines. The blocks were positioned iteratively by summing the source and background flux between pairs of OH lines and positioning the blocks sequentially such that the signal:noise improvement was maximised.

To calculate a rugate filter a genetic algorithm approach was used to optimise a refractive index profile of the form:

$$n(x < 0) = 1 \quad (1)$$

$$n(0 < x < x_0) = n_a + \sum_{i=1}^m \delta_i \sin(\alpha_i x + \phi_i) \quad (2)$$

$$n(x > x_0) = n_s \quad (3)$$

where  $n_s$  is the assumed refractive index of the substrate,  $n_a$  is the assumed average refractive index of the rugate film,  $m$  is the number of sinusoids included and  $x_0$  is the thickness of the film. The parameters,  $\alpha_i$ ,  $\delta_i$  and  $\phi_i$  were optimised using genetic algorithms.

Initially values of  $\alpha_i$ ,  $\delta_i$  and  $\phi_i$  were sought to maximise the function:

$$F = \left( 1 - \frac{\sum_{i=1}^{n_k} (T_{\text{filt}}(k_i) - T_{\text{ideal}}(k_i))^2}{n_k} \right) \quad (4)$$

where  $T_{\text{filt}}(k)$  is the calculated transmittance of the filter at a wavenumber  $k$  and  $T_{\text{ideal}}(k)$  is the predetermined ‘ideal’ transmittance profile. As the function began to converge the strategy was switched to seeking explicitly parameters that maximised some function of the relative improvement in the broad-band signal:noise ratio,  $G$ . To reflect the balance between the improvement in signal to noise ratio and the percentage of object flux retained ( $\tau$ ) an function of the form:

$$F = G^m \tau^n \quad (5)$$

was used where  $m$  and  $n$  are positive powers.

For a given refractive index profile the transmittance was calculated by dividing wavenumber space up into a series of discrete bins of width  $\delta k \approx 2 \times 10^{-3} \mu\text{m}^{-1}$  and approximating the continually varying refractive index profile by a series of thin homogeneous layers each with a constant refractive index. The transmittance at each value of  $k$  can then be calculated by the matrix method (Levi 1980). The transmittance profiles of the filters were calculated assuming a collimated beam at normal incidence. Throughout it was assumed that the filter materials were non-dispersive and absorption was assumed to be negligible.

The genetic algorithm approach is excellent at locating the region of the global minima (or maxima) in parameter

space, but the convergence to the exact minima (or maxima) is very slow and other optimisation techniques should be used to refine the solution (Goldberg 1989; Martin et al. 1995). A simple iterative optimisation technique was used to fine tune the solution some of the filter profiles. The filter was first converted from a series of layers with a stepped refractive index profile to an equivalent multilayer stack of high/low refractive index pairs. Southwell (1985) has shown that for thin layers ( $nt \ll \lambda$  where  $n$  is the refractive index and  $t$  the thickness), a single layer of intermediate refractive index can be replaced by two equivalent layers of high and low refractive indices with thickness given by:

$$t_{n_H} = t \left( 1 + \frac{n_H^2 - n_L^2}{n^2 - n_L^2} \right)^{-1} \quad (6)$$

$$t_{n_L} = t - t_{n_H} \quad (7)$$

By alternating the order of the equivalent layers ( $(n_H n_L)(n_L n_H)(n_H n_L) \dots$ ) this can be done without increasing the number of layers, provided the thin layer assumption holds. Provided the layers are sufficiently thin the new filter has the same transmittance properties as the original rugate filter. The resulting multilayer stack was optimised by choosing an initial step size,  $\delta t$  and looping over the layers, incrementing the thicknesses of the individual layers by  $\pm \delta t$ . For each layer the new fitness was calculated and if the change in thickness increased the fitness the change was retained. Once all the layers had been tested, if no change had been made to the filter the step size was decreased. Otherwise it was increased. The characteristic matrix of the filter is a product of the characteristic matrices of the individual layers. This property means that a simple optimisation scheme that sequentially tests and changes each layer can be implemented efficiently with the characteristic matrix at each step being given by:

$$\mathbf{C}_{filter}(t_i + \delta t) = \mathbf{C}_{1 \rightarrow i-1} \mathbf{C}_i(t_i + \delta t) \mathbf{C}_i^{-1}(t_i) \mathbf{C}_{i \rightarrow N} \quad (8)$$

where  $\mathbf{C}_i$  is the characteristic matrices of the  $i$ th layer and:

$$\mathbf{C}_{k \rightarrow j} = \left( \prod_{l=k}^j \mathbf{C}_l(t_l) \right) \quad (9)$$

Note that after the secondary optimisation, the filters are no longer true rugate filters in the sense that they no longer have continually varying refractive index profiles. However, they are derived directly from rugate filters.

#### 4 SIGNAL:NOISE IMPROVEMENT

The calculation of the signal:noise improvement followed the method given by Jones et al. (1997). The SNR without a filter is assumed to be:

$$(S : N)_0 = \frac{\epsilon S t}{(\epsilon t(S + B) + p(Dt + \sigma_R^2))^{1/2}} \quad (10)$$

where  $S$  is the integrated source flux,  $B$  is the integrated background flux (continuum plus line emission) both in electrons  $s^{-1}$  summed over the  $p$  pixels,  $D$  is the dark current ( $e^- \text{pix}^{-1} s^{-1}$ ),  $\sigma_R$  is the rms detector read noise ( $e^- \text{rms}$ ),  $p$  is the number of pixels illuminated by the source,  $\epsilon$  is the efficiency of the detector system and  $t$  is the exposure time in seconds. Following Jones et al. (1997), the introduction of the filter reduces the object flux to  $\tau S$  and the background flux to  $\beta B$ . The SNR becomes:

**Table 1.** Assumed Instrumental Parameters

|                               |  |
|-------------------------------|--|
| Telescope Diameter            | 3.9m   |
| System Efficiency, $\epsilon$ | 50%  |
| Image Scale                   | 0.5''/pixel  |
| Detector Read Noise           | J: 30e <sup>-</sup> rms<br>I: 1e <sup>-</sup> rms  |
| Dark Current                  | J: 5e <sup>-</sup> pix <sup>-1</sup> s <sup>-1</sup><br>I: 0e <sup>-</sup> pix <sup>-1</sup> s <sup>-1</sup> |
| Quantum Efficiency            | J: 70%   |
| size of source                | I: 90% @ < 0.85 $\mu$ m, 60% @ 0.95 $\mu$ m<br>0.5'', 1'', 2''   |

$$(S : N)_F = \frac{\epsilon \tau S t}{(\epsilon t(\tau S + \beta B) + p(Dt + \sigma_R^2))^{1/2}} \quad (11)$$

The improvement (or otherwise) in the signal:noise ratio is given by:

$$\frac{(S : N)_F}{(S : N)_0} = \tau \left( \frac{\gamma + 1 + k(t, B)}{\tau \gamma + \beta + k(t, B)} \right)^{1/2} \quad (12)$$

where  $k(t, B)$  is a function of  $t$  and  $B$  that is independent of the filter parameters and  $\gamma = S/B$ . The assumed instrument parameters are listed in Table 1. For the  $J$  band a constant quantum efficiency of 70% was assumed with a read noise of 30e<sup>-</sup> and dark current of 5e<sup>-</sup>s<sup>-1</sup>. The assumed read noise in  $J$  is conservative and modern CCD's can have a read noise as low as 5e<sup>-</sup> but the values were chosen to be consistent with previous calculations (Jones et al. 1997). For the  $I$  band the quantum efficiency curve of an MITLL-CCD deep depletion device was assumed. This gives a QE of around 90% at wavelengths less than 0.85 $\mu$ m dropping to around 60% at 0.95 $\mu$ m. A read noise of 1e<sup>-</sup> and negligible dark current were assumed.

In order to keep the calculations as general as possible continuum sources were used throughout. For the  $J$  band a continuum source with a magnitude of 22 was assumed. The flux was calculated using the zero magnitude values of Koornneef (1983). This gave a total flux of 47 photons s<sup>-1</sup> m<sup>-2</sup> arcsec<sup>-2</sup> band<sup>-1</sup> which was assumed to be constant across the band.

It is also necessary to estimate the background flux across the band. Maihara et al. (1993) quote a night sky continuum of about 560 photons s<sup>-1</sup> m<sup>-2</sup> arcsec<sup>-2</sup>  $\mu$ m<sup>-1</sup> measured at 1.65  $\mu$ m. The continuum is expected to be less at shorter wavelengths and a night sky continuum of 300 photons s<sup>-1</sup> m<sup>-2</sup> arcsec<sup>-2</sup>  $\mu$ m<sup>-1</sup> was assumed (Sobolev 1978). This gave a  $J$  band total of 72 photons s<sup>-1</sup> m<sup>-2</sup> arcsec<sup>-2</sup> band<sup>-1</sup>. The  $J$  band emission line data used by Jones et al. (1997) was used (Piché 1996). The emission lines were represented by Gaussians of width 1 $\text{\AA}$  centred at the line locations, such that the integrated flux was equal to the line intensity. The total flux from emission lines in the  $J$  band was 3560 photons s<sup>-1</sup> m<sup>-2</sup> arcsec<sup>-2</sup> band<sup>-1</sup>.

For the  $I$  band calculation an  $I$  band centred at 0.84 $\mu$ m with a FWHM of 0.239 $\mu$ m and a zero magnitude flux of  $9.9 \times 10^{-10}$  erg cm<sup>-2</sup> s<sup>-1</sup>  $\text{\AA}^{-1}$  was assumed. This extends further into the red than many conventional  $I$  filters and covers a substantial portion of the spectrum included in  $z$  filters (see for example Fukugita et al. (1996)). A continuum source of magnitude 24 was used. The night sky in the  $I$  band is much less intense than in the  $J$  band, with a magnitude > 19

arcsec<sup>-2</sup> compared with about 15 arcsec<sup>-2</sup> for the *J* band. In particular the OH emission is much weaker. The vibrational transitions giving rise to the *I* band OH emission change the OH vibrational quantum number,  $\nu$ , by  $\Delta\nu = 4$  and  $\Delta\nu = 5$ . The *J* band OH emission is from  $\Delta\nu = 3$  transitions. The transition probability falls off rapidly with increasing  $\Delta\nu$  (Bates 1982) with the consequence that the *I* band OH lines are much fainter. For example, Harrison and Kendall (1973) measured a total intensity for the seven principle OH bands between 0.72 and 0.96 $\mu\text{m}$  that was roughly one tenth of the intensity measured for the three principle OH bands in the *J* photometric band. Llewellyn (1978) predicted a similar intensity distribution.

Estimation of the intensity of the OH lines is one of the major uncertainties in all these calculations. The intensities are highly variable and poorly known in all wavelength bands. The positions and relative intensities of the *I* band OH lines at wavelengths less than 0.94 $\mu\text{m}$  were taken from a fit to a high resolution spectrum kindly obtained for us by C.G. Tinney with the CASPEC echelle at the ESO 3.6m telescope. The data were obtained in a 6900 sec exposure at 9 km s<sup>-1</sup> resolution during dark time. The absolute intensities were scaled so that the total intensity of the OH bands and the 0.865 $\mu\text{m}$  oxygen band equalled the total intensity measured by Johnston & Broadfoot (1993) at an altitude of 2750m and latitude of 32°26.6'N. The band intensities measured by Johnston & Broadfoot (1993) are approximately half the band intensities measured by Harrison & Kendall (1973) but are similar to, or slightly larger than, the predicted intensities calculated by Llewellyn et al. (1978). The line positions of the band around 0.945 $\mu\text{m}$  were taken from the spectra of Abrams et al. (1994) and Osterbrock et al. (1997) and the relative intensities were estimated from the spectra of Osterbrock et al. (1997) and Steed & Baker (1978). The lines were scaled so that the total intensity was equal to that calculated by Llewellyn et al. (1978). This gave a total of 152 line photons s<sup>-1</sup> m<sup>-1</sup> arcsec<sup>-2</sup> between 0.65 and 0.96 $\mu\text{m}$ .

Since the *I* band OH lines are weaker than in *J*, the value of the background continuum is more critical in the signal to noise ratio calculations, but it's value is equally as uncertain as the *J* band value. Noxon (1978) measured 130 photons s<sup>-1</sup> m<sup>-2</sup> arcsec<sup>-2</sup>  $\mu\text{m}^{-1}$  at 0.85 $\mu\text{m}$  in a dark sky and this was the value adopted for the calculations. It was assumed that the continuum was flat, giving 40 continuum photons s<sup>-1</sup> m<sup>-1</sup> arcsec<sup>-2</sup> in the same wavelength range. The resulting *I* band sky spectrum gave a magnitude of 19.9 arcsec<sup>-2</sup> which is consistent with dark sky measurements in the *I* band.

For both the *I* and *J* bands, the total source and background fluxes were multiplied by the atmospheric transmission as a function of wavenumber and binned into a discrete grid in wavenumber space.

The improvement in signal to noise ratio has been calculated assuming equal exposure times with and without the filter. If the exposure time is limited by sky saturation, the maximum improvement in signal to noise ratio for a single exposure is potentially much higher. If  $t$  is the time taken before saturation without the filter, then the exposure times with the filter can be increased to  $t' = t/\beta$ . The resulting improvement in S:N for a single exposure is:

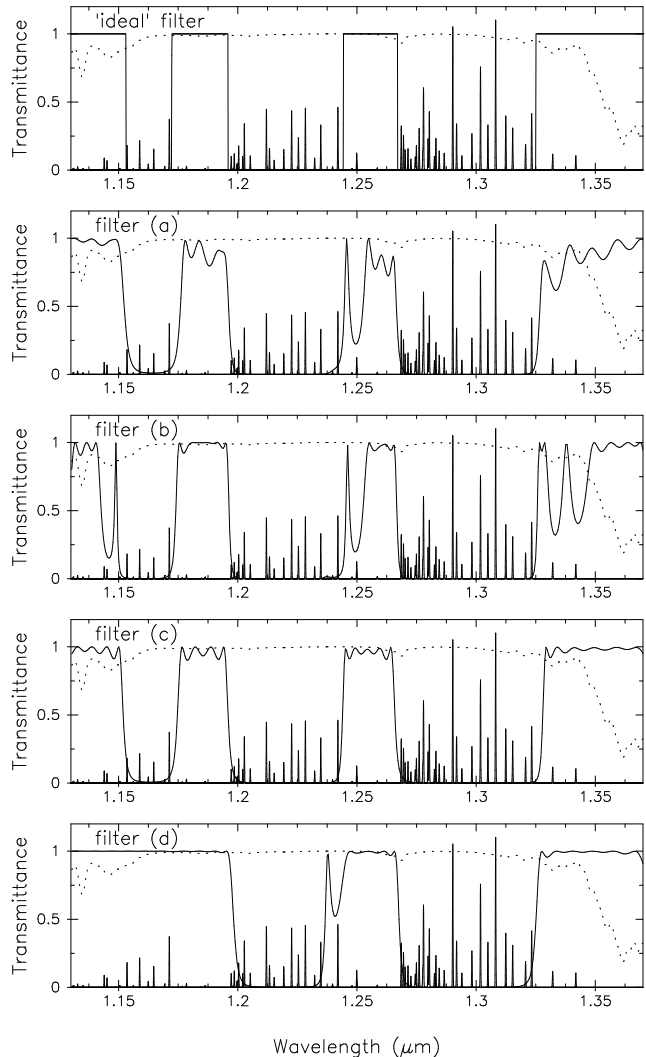


**Figure 2.** The transmittance profiles as a function of wavelength for the ‘ideal’ filter and filters (a) to (d) described in the text. The positions of the emission lines and the atmospheric transmittance profile are also shown.

$$\frac{(S:N)_F(t/\beta)}{(S:N)_0(t)} \approx \frac{1}{\beta^{1/2}} \frac{(S:N)_F(t)}{(S:N)_0(t)} \quad (13)$$

## 5 CALCULATIONS AND RESULTS

### 5.1 J-band Filter

The OH lines in the *J* band are shown in figure 1. The bands fall into three distinct regions so an ‘ideal’ blocking filter with three blocking bands was chosen. The ‘ideal’ blocking filter is shown in figure 2. This filter increases the broadband signal to noise ratio for a 1'' magnitude 22 source by a factor of 2. Higher gains are possible with more and finer blocking lines. However, for the sake of illustration, we chose to keep the filter relatively simple at this stage.

Using the ‘ideal’ filter as an initial template, four filters were derived whose transmittance profiles are also shown in figure 2. The transmittance calculations assumed a collimated beam at normal incidence. The properties of these

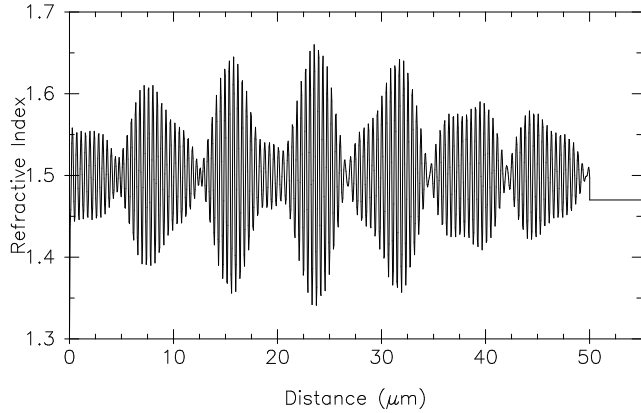


**Figure 3.** The Refractive Index Profile for Filter (a)

filters are summarised in table 2. All filters assumed a substrate refractive index of 1.47. Filter (a) is a true rugate filter designed by GA alone. The RI profile is the sum of 10 sinusoids constrained to lie between  $\alpha = 4\pi n_a / (1.39\mu\text{m})$  and  $\alpha = 4\pi n_a / (1.12\mu\text{m})$  with no constraint on the minimum and maximum allowed refractive index. It was designed to minimise the function  $G^4\tau^{1/4}$  where  $G$  is the factor by which the signal to noise ratio is increased. The narrow dips in the transmittance corresponding with the outlying emission lines are a feature of the GA optimisation. The resulting refractive index profile is shown in figure 2. It covers a range of 1.34 to 1.66. With a small amount of clipping which does not degrade the transmittance profile, it is within the range allowed by real materials (eg 1.35 (cryolite) and 2.3 (ZnS)).

Filters (b) and (c) resulted from further optimisation of the GA solution shown in figure 2. The optimisation technique described in section 3 converts the sinusoidal profiles into multilayer stacks so the resulting filters are no longer true rugate filters although they derive directly from them. The optimisation process is illustrated in figure 3. The first panel shows the clipped 50 $\mu\text{m}$  thick rugate filter from which filters (b) and (c) were derived. For illustration, a minimum and maximum refractive index of 1.35 and 1.62 was imposed (eg. cryolite, alumina). The materials were assumed to be non-dispersive and absorption was assumed to be negligible. The sinusoidal profile was approximated by a series of 0.1 $\mu\text{m}$  thick homogeneous layers shown in part in the second panel. These in turn were translated into a stack of high/low refractive index layers (third panel). The final panel shows the same section of filter (b) after optimisation. Filter (b) was optimised to maximise the function  $G^4\tau$  and filter (c) was optimised directly to fit the ‘ideal’ transmittance profile.

Filter (d) in contrast was chosen to illustrate the balance between spectral coverage and improved sensitivity. It was produced by matching to an ‘ideal’ transmittance profile with only two blocking bands.

The results of the signal to noise calculations for the four filters are summarised in table 3 and illustrated in figures 5 and 6. Table 3 gives the detailed results for a magnitude 22 continuum object. Figure 5 shows the calculated signal to noise ratio for filters (a) to (d) and for no OH suppression (solid line) as a function of object magnitude assuming a 1'' continuum source. Figure 6 illustrates the increase in exposure time before the detector saturates as-

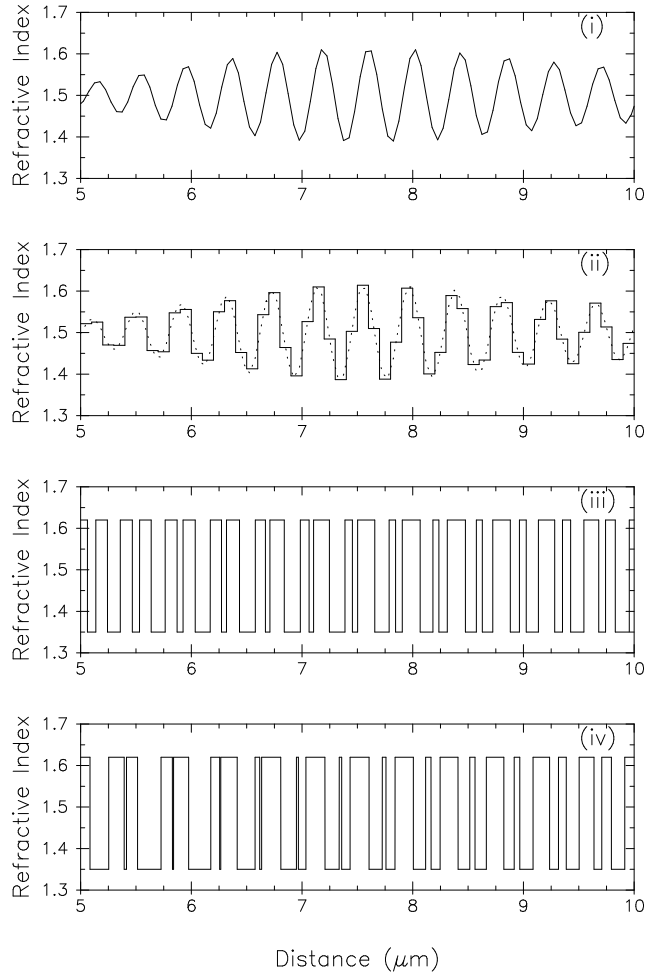


**Figure 4.** Steps in the further optimisation of the GA results: (i) an enlarged section ( $x = 5 \rightarrow 10\mu\text{m}$ ) of the clipped version of the refractive index profile of filter(a) from which filters (b) and (c) were derived; (ii) an approximation to (i) with 0.1 $\mu\text{m}$  homogeneous layers; (iii) conversion of (ii) into high/low refractive index stack; (iv) the result of optimisation (filter b).

suming a 1'' magnitude 22 object and pixel saturation at  $10^5$  electrons.

It can be seen that all rugate filters offer significant improvements over standard photometric bands in terms of the increase in signal to noise ratio for faint sources, with a factor of two improvement in signal to noise ratio for filter (b). Improvements in signal to noise ratio are possible for sources fainter than about magnitude 15 for a 2'' source, 16.5 for a 1'' source and 18 for a 0.5'' source. A secondary advantage is the increase in exposure times allowed, with maximum exposure times increasing by a factor of 30 for filter (b).

Filter (b), optimised to a function of the form  $G^n\tau^m$ , gives the best performance in terms of both the increase in signal to noise ratio and the increased exposure time allowed but this is at the expense of the spectral coverage. Filter (c) retains a greater percentage of the object flux, at 44% and still gives a significant improvement in the signal to noise ratio. The transmittance profile of filter (c) is more feasible in practice than filters (a) and (b). Broad features will be less affected by small deviations in the refractive index

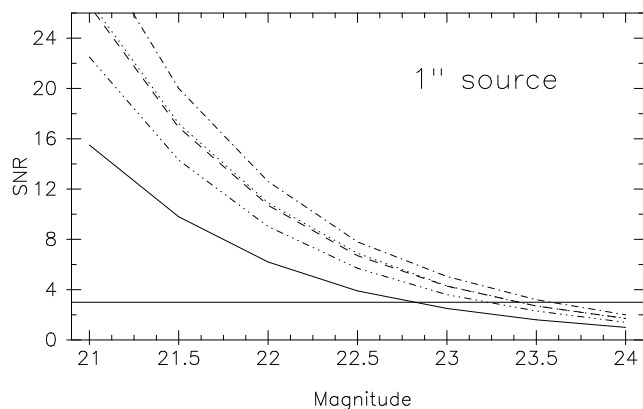
**Table 2.** Summary of Filter Properties

| Filter | Description                            | Average RI | Min RI | Max RI | Thickness       | No. of Layers |
|--------|--|------------|--------|--------|-----------------|---------------|
| Ja     | True rugate maximising $G^4\tau^{1/4}$ | 1.5        | 1.34   | 1.66   | $50\mu\text{m}$ |               |
| Jb     | Optimised to maximise $G^4\tau$        | 1.5        | 1.35   | 1.62   | $50\mu\text{m}$ | 500           |
| Jc     | Optimised to 'ideal' filter            | 1.5        | 1.35   | 1.62   | $50\mu\text{m}$ | 500           |
| Jd     | Optimised to maximise $G\tau$          | 1.5        | 1.35   | 1.62   | $50\mu\text{m}$ | 500           |
| I      | Optimised to 'ideal' filter            | 1.5        | 1.35   | 1.62   | $50\mu\text{m}$ | 500           |

**Table 3.** Improvement in Signal to Noise Ratio for a 600s integration time. Results are given for objects of magnitude  $J = 22$  and  $I = 24$ .

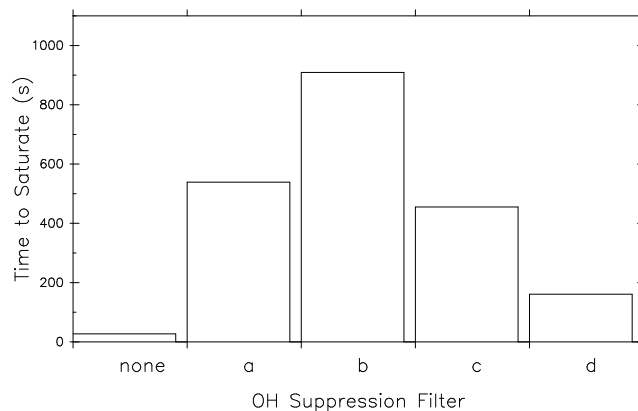
|              | $G$   |             | $\tau$  | $\beta^{(a)}$ |
|--------------|-------|-------------|---------|---------------|
| source size: | $2''$ | $1''$       | $0.5''$ |               |
| 'Ideal' J    | 2.04  | <b>2.03</b> | 1.98    | 0.47          |
| Filter (Ja)  | 1.74  | <b>1.73</b> | 1.69    | 0.40          |
| Filter (Jb)  | 2.05  | <b>2.03</b> | 1.97    | 0.36          |
| Filter (Jc)  | 1.76  | <b>1.75</b> | 1.72    | 0.43          |
| Filter (Jd)  | 1.46  | <b>1.46</b> | 1.45    | 0.60          |
| 'Ideal' I    | 1.23  | <b>1.21</b> | 1.15    | 0.45          |
| Filter (I)   | 1.17  | <b>1.16</b> | 1.12    | 0.50          |

<sup>a</sup>  $1/\beta$  is approximately the factor by which the maximum exposure time before saturation is increased in the sky dominated limit


**Figure 5.** The signal to noise ratio as a function of magnitude for a  $1''$  with no OH suppression (solid line) and with the four filters (dashed line: filter (a); dash-dot: filter (b); dotted line: filter (c) and dash-dot-dot-dot: filter (d)).

profile and departure from normal incidence than narrow dips aligned with individual OH lines.

Filter (d) gives a far better spectral coverage than the other three filters with 60% of the object flux being retained. This is at the expense of some loss in sensitivity with a signal to noise improvement of 1.45 for a  $1''$  magnitude 22 continuum object. However, the relatively large fraction of line emission retained limits the increase in maximum exposure time and implies that the filter performance will be far more dependent on the intensity of the OH lines, which is a highly variable and uncertain quantity.


**Figure 6.** The time until saturation (assuming saturation at  $10^5$  electrons/pixel) for no OH suppression and for the four  $J$  band OH suppression filters discussed.

## 5.2 I band filter

The OH lines in the  $I$  band were shown in figure 1. The OH bands at the long wavelength end of the band are well separated, but the windows between the bands are no longer so clear. In particular, there is a relatively intense oxygen band around  $0.865\mu\text{m}$ . At shorter wavelengths the bands are less intense but overlap so again the windows between bands are not so clean.

Figure 7 shows the  $I$  band equivalent of filter Jc. As for the  $J$  band filters, the transmittance profile has been calculated assuming a collimated beam at normal incidence, and assuming non-dispersive materials. A substrate refrac-

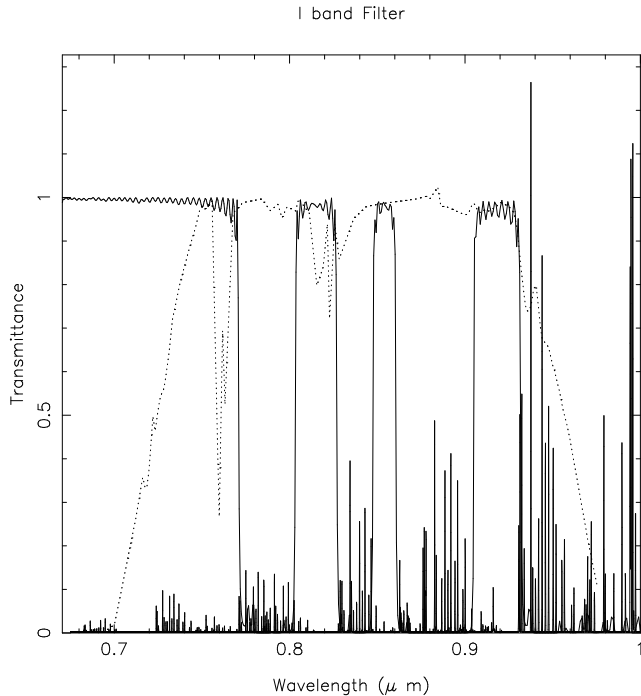


**Figure 7.** The transmittance profile as a function of wavelength for an I band OH suppression filter. The dotted line is a product of the atmospheric absorption and the assumed I band profile.

tive index of 1.47 was assumed and the initial refractive index profile, expressed as a sum of ten sinusoids, varied between 1.30 and 1.71. This was truncated at 1.35 to 1.62 before the final optimisation. The properties of the filter are summarised in table 2.

The improvement in signal to noise ratio was calculated for a magnitude 24 continuum object, and the results are summarised in table 3. The corresponding values of the signal to noise ratio for a 600s integration time and a magnitude 24 1'' continuum object are 9.2 with no OH suppression and 10.6 with the OH suppression filter. As can be seen, the results are much less spectacular than for the *J* band, although a small improvement in signal to noise ratio of a factor of 1.16 can still be found. Greater improvements in signal to noise ratio are possible but with increasingly complex transmission profiles. The relatively poor performance is partly a result of the distribution of line emission in the band but largely a result of the relatively high fraction of the background intensity in the continuum. Note that the improvement in the signal to noise ratio depends on the balance between the background line and continuum intensities. The values chosen here are conservative. If the continuum is completely neglected than the improvement in signal to noise ratio for a magnitude 24 1'' continuum object rises to 1.39, suggesting a potential 39% improvement in the signal to noise ratio if the continuum is very small compared with the intensity of the emission lines.

## 6 DISCUSSION

### 6.1 Filter Manufacture

The major challenge of the rugate technology has been to develop design software compatible with the control systems of vacuum deposition chambers. Coating designs which can be expressed as the sum of up to a dozen sine waves appear to be the most straightforward to manufacture. But it should be stressed that the technology is sufficiently new that filter transmission profiles as complex as those proposed in Fig. 2 have not been attempted by commercial companies before. A constraint imposed at the outset was to limit the optical coating thickness to  $\approx 20\mu\text{m}$ , and infrared coatings to  $\approx 40\mu\text{m}$ , since thicker coatings are a major technical challenge. Even these limits are at least twice the thickness of routine multilayer coatings used in interference filters. At the outset, the number of layers, and hence the coating thickness, relates almost directly to how long the filter resides within the vacuum chamber. Interference filters are produced with real-time quality control and it becomes more difficult to control the transmissive behaviour as more layers are laid down.

Motivated by our designs, B. Bovard has demonstrated with a combination of tantalum pentoxide ( $n_o = 1.5$ ) and silicon dioxide ( $n_o = 2.3$ ) that the desired filter response in Fig. 2ii can be achieved with a  $40\mu\text{m}$  thickness rugate coating. The narrowest rejection band at 1170nm drives the total coating thickness; the broad rejection bands are much less challenging. For the  $\text{Ta}_2\text{O}_5:\text{SiO}_2$  refractory oxide combination, the troughs achieve blocking to better than 0.1% while the peaks have steep sides and average better than 90% transmission. He finds the central wavelength of each rejection band can be achieved to within 1%, but the width is more uncertain by as much as 5% of the rejection band. Bovard has achieved optical quality and a uniform spectral response over a 150mm diameter and suggests that a 200mm diameter is within reach. Rugate coatings require intricate (mostly proprietary) deposition techniques carried out with great care over several days in a vacuum chamber. This makes them expensive with costs per filter close to  $\sim\text{US}\$30,000$ , although possible approaches to reducing costs include subdividing a coated blank with a diamond pencil.

It has been shown that effective *J* band OH suppression filters can be designed in principle but the robustness of such a filter is an important consideration in practice. There are several effects which serve to degrade filter performance. Thermal effects induce a bandpass shift at the level of  $0.2\text{\AA K}^{-1}$ . Small corrections are possible with filter tilts if the original filter is specified at a temperature warmer than under observing conditions. Deviations from optical flatness are caused by microstructure within the coatings and by bowing in the filter substrate due to strong surface tension (stress) within the coating dielectric (Ennos 1966; Martin et al. 1991). Basic approaches to reduce bowing are to apply the coating layers to both sides of the substrate, or to bind the multilayer coating to a thick ( $\sim 10\text{mm}$ ) substrate, but a large optical thickness can seriously degrade the optical performance of the camera. An alternative route is to match materials with tensile and compressive stress (e.g. zinc sulphide:cryolite, zinc sulphide:thorium fluoride). This contrasts with Bovard's hard coating where both dielectrics



are compressive, a combination which has proven stability and longevity.

Small differences in manufacture induce in situ stress across the plates, although ion bombardment can remedy this to some degree (Martin et al. 1991). Deviations from optical flatness cause the filter peaks to spread, thereby filling in the troughs.

The performance of the filter when expressed as an improvement in the signal to noise ratio has a highly complicated dependence on the transmittance profile. Some insight into the sensitivity of the signal to noise improvement to the degradation of the filter profile can be gained by fitting Butterworth functions to the low transmittance notches in the ‘ideal’  $J$  filter profile shown in figure 2*i*. The Butterworth profile is given by:

$$f_n(\lambda) = \left( 1 + \left( \frac{\lambda - \lambda_c}{h/2} \right)^{2n} \right) \quad (14)$$

where  $\lambda_c$  is the central wavelength of the notch and  $h$  is the FWHM (full width at half max) of the function. Figure 8 shows three Butterworth functions with the same FWHM and central wavelength as the square notches in figure 2*i* but with  $n = 3, 6, 10$  and  $30$ . A square profile results when  $n \rightarrow \infty$ . By varying  $n$  and  $h$  the Butterworth functions can be used to model the effects of both changes in the width of the notches and increasing roundness of the notches. Figure 9 shows the variation in the improvement in signal to noise ratio as a function of incremental change in the half width of the three notches in figure 8 for  $n = \infty$  (square wave profile), and  $n = 3, 6, 10$  and  $30$ . A degradation of the profile through small irregularities would both smooth the profile (ie decrease  $n$ ) and change the half width so extrapolation to a real degraded filter is difficult. However, it can be seen that the signal to noise improvement is more tolerant to a broadening of the notches (increase in halfwidths) than to a narrowing of the notches. The percentage background intensity retained can increase rapidly as the notch shrinks and additional strong OH lines are admitted. The percentage drop in object flux resulting from a broader notch is much smaller than the percentage rise in background resulting from a narrow notch.

## 6.2 Instrumental Applications

Up to this point, our calculations have assumed a collimated beam at normal incidence. However, wide field imaging surveys are carried out with fast cameras in which blocking filters are traditionally used in the converging beam. It is well known that such beams modify both the first and second moments of the filter transmission profile. The former is rectified by shifting the desired filter response to red wavelengths at the design stage. The latter limits the speed of the beam depending on the precise filter structure and the angle subtended by the detector seen from the camera lens. Analytic approximations to the first four moments are given by Bland-Hawthorn (1997). We find that the rugate profiles presented in Fig. 2 suffer negligible degradation in beams slower than  $f/3$ , inclusive of non-telecentric rays over a  $20'$  field.

The new-generation Rockwell HAWAII arrays provide high (60%) quantum efficiency in the near-infrared with

Butterworth profile fits with  $n=3,6,10$  and  $30$

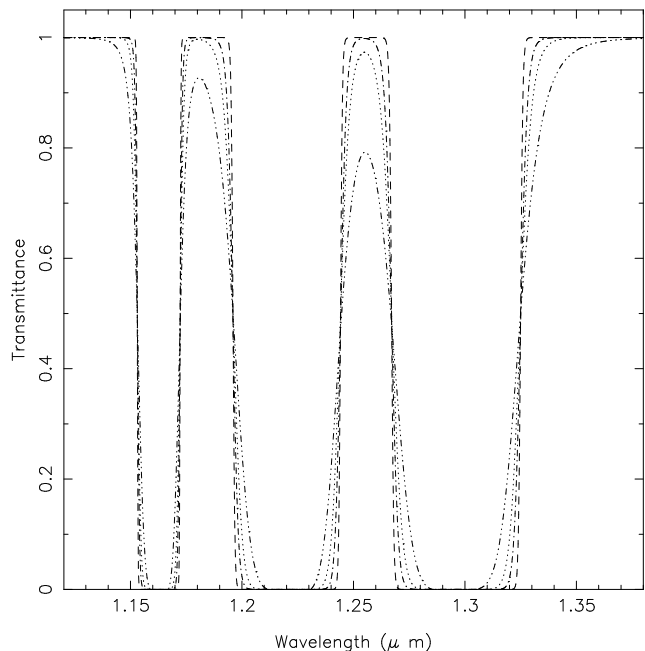


**Figure 8.** Butterworth profiles with the same central wavelengths and half widths as the notches in the ‘ideal’  $J$  filter but with  $n = 30$  (dashed line),  $n = 10$  (dot-dash),  $n = 6$  (dotted) and  $n = 3$  (dash-dot-dot-dot).

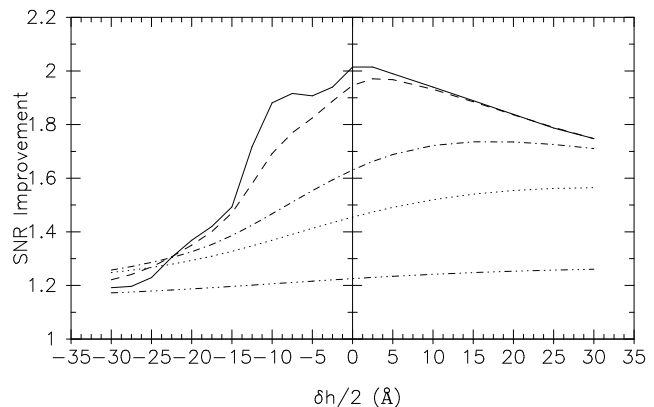


**Figure 9.** The variation of signal to noise improvement as a function of the incremental change in the half widths of Butterworth profiles with  $n = \infty$  (solid line),  $n = 30$  (dashed line),  $n = 10$  (dot-dash),  $n = 6$  (dotted line) and  $n = 3$  (dash-dot-dot-dot). When  $\delta h = 0$  these correspond to the transmittance profiles shown in figure 8. Positive  $\delta h$  corresponds to broader low transmittance notches.

moderate performance (50%) in the  $I$  and  $z$  bands. An optical system built around a HAWAII array could achieve comparable sensitivity in standard  $I$  and rugate  $J$  bands. Such a device could also capitalize on an  $IzJ$  filter to enhance the sensitivity at near infrared wavelengths compared to conventional optical bands. For example, figure 10 illustrates a transmission profile that will reduce the sky background for  $\lambda > 1\mu\text{m}$  to the same level as the sky background for  $\lambda < 1\mu\text{m}$ , thereby allowing a relatively uniform  $IzJ$  band to be defined. Clearly this profile also incorporates an extended

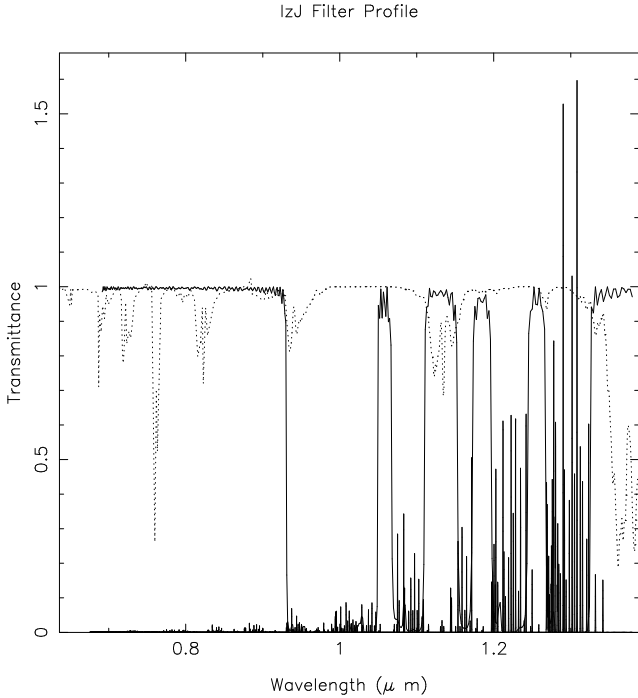


**Figure 10.** A transmittance profile as a function of wavelength for an  $IzJ$  filter that would reduce the sky background in  $J$  to the same level as in  $I$ . The dotted line is the atmospheric transmittance.

$J$  or  $zJ$  filter from 1.05 to  $1.38\mu\text{m}$  which gives access to an additional clean spectral window not used in the  $J$  filters discussed earlier.

A very different application of rugate technology would be to devise a beam splitter whose complementary images amplify some characteristic in the spectrum of a class of objects. This idea, discussed in the next section, has the potential to usher in a spate of inexpensive astronomical imagers as the technique can be exploited with a rudimentary optical design.

### 6.3 Scientific Applications

Rugate filters are expected to increase observing efficiency at most sites, and therefore the scientific applications are numerous. One example, discussed further below, is very low mass (VLM) stars and brown dwarfs. These are so rare and faint that they require dedicated surveys over huge volumes – which means either very wide field or very deep surveys. The most reliable survey diagnostic is the  $I - J$  colour (Leggett 1992), which is exactly the wavelength range where rugate technology will produce the largest gain in sensitivity.

For continuum sources, we have seen that signal:noise gains as high as 2 are possible in the rugate  $J$  band. This may find important uses in studies of galaxy evolution since the K-corrections at  $J$  are much closer to those at  $K$  (Fig. 11) than to optical bands (Glazebrook 1997). In particular, the K-corrections for the different morphological classes are remarkably uniform for rugate filters  $Jc$  and  $Jd$  over the redshift interval  $z = 1 - 3$ . Thus, evolutionary signatures should be much easier to monitor in a rugate  $J$  filter than at  $I$ , and the higher sensitivity at  $J$  compared to  $K$  makes it the

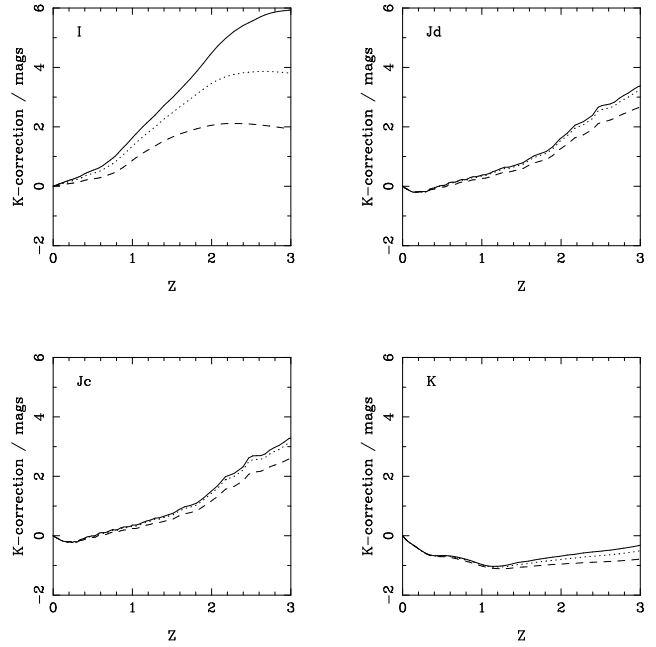


**Figure 11.** K-corrections at  $I$  and  $K$  compared to two rugate filter designs,  $Jc$  and  $Jd$  (see Fig.2). The galaxy types shown are elliptical galaxies (solid lines), early-type spirals (dotted lines), and late-type/irregular spirals (dashed lines). The small bumps on the rugate curves are due to the H,K break moving through the sub-bands.

preferred near-infrared band out to at least  $z = 2$ . The morphological types start to diverge when the H,K break enters the band: this occurs at  $z = 1$  for  $I$  and  $z = 2$  for  $J$ . The K-corrections for the rugate filters are remarkably stable as they agree to 0.1 mag out to  $z = 3$ .

Even larger gains are possible in observations of emission-line sources, assuming that the spectral line falls within one of the transmitting windows. If the object signal arises in a discrete, narrow interval transmitted by the filter, no signal from the object is lost by the OH suppressing bands, in which case signal:noise gains as high as 4 are possible. In redshift surveys, roughly half of the survey volume is lost to the suppressing bands, although this overstates the problem if the line-emitting source transmits in several bright lines within the broad window. To date, searches for high redshift galaxies have concentrated on only a few strong lines from  $\text{Ly}\alpha$  to  $\text{H}\alpha$ . In Table 4, we show the transmitted redshift ranges for three prominent emission lines. The redshift slices transmitted by rugate filter  $Jc$  are well matched to the redshift range over which the star formation rate density is expected to peak in the early universe (Ellis 1997).

We reiterate a point made by Jones et al. (1997) that in circumstances where a rugate filter does not produce a substantial gain, this may still be the preferred option due to the longer exposure times and suppressed background variation between exposures. It is anticipated that this will lead to much better image mosaics than have been possible to date.

This paper has concentrated on the use of rugate filters for OH suppression but the great versatility of rugate technology could find many uses within astronomy. For example, in the case of brown dwarfs the ability to define ir-

**Table 4.** Rugate filter *J*c: transmitted redshift ranges for prominent emission lines

| H $\alpha$ | [OIII]5007 | [OII]3727 |
|------------|------------|-----------|
| 0.71-0.76  | 1.24-1.30  | 2.01-2.09 |
| 0.79-0.82  | 1.34-1.39  | 2.14-2.21 |
| 0.90-0.93  | 1.49-1.53  | 2.34-2.40 |
| 1.02-1.09  | 1.65-1.74  | 2.56-2.68 |

regular bands within a single filter suggests an alternative approach to finding these elusive objects. At near-infrared wavelengths, the spectrum of Gliese 229B (Geballe et al. 1996) has a roughly sawtooth appearance. A rugate filter could be made to operate as a beam splitter such that the peaks of the sawtooth are transmitted and the troughs are reflected by the filter. If the separate paths are imaged onto two detectors, candidate objects would appear bright in one image and dark at the same location on the other detector. The graded index coatings are sufficiently flexible that the precise positions of the peaks and troughs could be chosen to share the sky background equally between both filters. Thus, rugate technology could give rise to a range of niche instruments designed to find specific classes of astrophysical objects with distinctive spectra.

In summary, interference filters offer a practical approach to achieving significant gains in OH-suppressed imaging. We recognise that more sophisticated techniques could be conceived. One possibility is the use of an OH absorption cell to absorb the OH line emission directly. But the production and maintainance of a vibrationally excited OH population with a sufficiently high column density would be a major technical challenge. The vibrational bands contributing in the *J* band are the  $\nu = 8 \rightarrow 5$ ,  $7 \rightarrow 4$  and  $6 \rightarrow 3$  bands, thus OH of vibrational levels at least up to  $\nu = 5$  would be required at relatively high concentrations. Relaxation of the vibrational states would rapidly depopulate the higher vibrational levels and some means of maintaining the vibrationally excited population would be required (Kondratyev 1969). This simple idea is likely to prove complex and costly to implement. Although less elegant, the OH suppression filters can be produced relatively cheaply with existing technologies and could easily be incorporated into conventional instruments.

## 7 SUMMARY

The sensitivity of astronomical observations in the near infrared is limited by the presence of intense atmospheric OH emission bands. The conventional approach to improving sensitivity has been to increase the telescope aperture. However, in limited cases, noise reduction can achieve major gains in sensitivity. In this paper we have shown that the simulated rugate filters can achieve extraordinary gains for imaging at *J*, and modest gains through *I* and *z*, at the expense of loss in bandpass. A similar *H* band filter would require a much more complicated transmission profile and, since the transmission profiles proposed for the *I* and *J* bands are already near the limit of currently realisable profiles, it was not considered in detail. Plans are already well advanced to manufacture a rugate *J* filter for wide field

imaging at the Anglo-Australian 3.9m Telescope. We have provided examples of astrophysical studies that will clearly benefit from such a filter, as we propose to demonstrate in subsequent papers.

## 8 ACKNOWLEDGEMENTS

We are indebted to K. Glazebrook for producing Fig. 11 and for helpful dialogues throughout the work. We would also like to thank P.A. Markham, I.J. Lewis and C.G. Tinney for useful comments. On the technical aspects, R.P. Netterfield and B.G. Bovard offered constructive advice at critical stages of the work. We acknowledge the stimulating atmosphere at the Anglo-Australian Observatory which has sustained much of the development work described here.

## REFERENCES

- Abrams M.C., Davis S.P., Rao M.L.P., Engleman R.Jr., Brault J.W., 1994, ApJS, 93, 351  
 Bates D.R. & Nicolet M., 1950, JGR, 55, 301  
 Bates D.R., 1982, in Massey H.S.W. & Bates D.R., eds, Atmospheric Physics and Chemistry v1, Applied Atomic Collision Physics, 149  
 Bland-Hawthorn J. 1997, PASP, submitted  
 Broadfoot A.L. & Kendall K.R., 1968, JGR, 73 426  
 Charbonneau P. , 1995, ApJS, 101, 309  
 Content R. 1996, ApJ, 464, 412  
 Content R. & Angel R., 1994, in Crawford D.L. and Craine E.R., eds, Proc. SPIE 2198, Instrumentation in Astronomy VIII, 757  
 Dobrowolski, J.A. & Verly, P.G., eds, 1993, Proc.SPIE. 2046, Inhomogeneous and Quasi Inhomogeneous Optical Coatings  
 Ellis R.S. 1997, Annual Reviews, 35, in press (astro-ph/9704019)  
 Ennos A.E. 1966, Appl.Opt. 5, 51  
 Fabricus H. 1992 Appl.Opt. 31 5191  
 Fukugita M., Ichikawa T., Gunn J.E., Doi M., Shimasaku K. & Schneider D.P., 1996, AJ, 111, 1748  
 Geballe T.R., Kulkarni S.R., Woodward C.E. & Sloan, G.C. 1996, ApJ, 467, 101  
 Glazebrook K., 1997, in Mamon G.A., Thuan T.X. & Van J.T.T., eds, Extragalactic Astronomy in the Infrared, Editions Frontieres  
 Goldberg D.E., 1989, Genetic Algorithms, Addison-Wesley  
 Greiner H. , 1996, Appl.Opt., 35, 5477  
 Harrison & Kendall, 1973, Planet.Space.Sci., 21, 1731  
 Herbst T.M. , 1994, PASP, 106, 1298  
 Iwamuro F., Maihara T., Oya S., Tsukamoto H., Hall D.N.B., Cowie L.L., Tokunaga A.T. & Pickles A.J., 1994, PASJ, 46, 515  
 Johnson W.E. & Crane R.L., 1993, in Dobrowolski, J.A. & Verly, P.G., eds, Proc.SPIE.2046, Inhomogeneous and Quasi Inhomogeneous Optical Coatings, 88

- Johnston J.E. & Broadfoot A.L., 1993, JGR, 98(A12), 21593  
 Jones D.H., Bland-Hawthorn J. & Burton M.G., 1996, PASP, 108, 929  
 Kondratyev K.Ya., 1969, Radiation in the Atmosphere, Academic Press, New York and London  
 Koorneef J. 1983, A&A, 128, 84  
 Leggett, S.K. 1992, ApJS, 82, 351  
 Le Texier H., Solomon S. & Garcia R.R., 1987, Planet.Space.Sci. 35, 977  
 Levi L., 1980, Applied Optics: A Guide to Optical System Design v2, Wiley Interscience, chapter 11  
 Llewellyn E.J., Long B.H. & Solheim B.H., 1978, Planet.Space.Sci., 26, 525  
 Maihara T., Iwamuro F., Yamashita T., Hall D.N.B., Cowie L.L., Tokunaga A.T., & Pickles A., 1993, PASP, 105, 940  
 Maihara T., Iwamuro F., Oya S., Tsukamoto H., Hall D.N.B., Cowie L.L., Tokunaga A.T., & Pickles A.J., 1994, in Crawford D.L. and Craine E.R., eds, Proc. SPIE 2198, Instrumentation in Astronomy VIII, 194  
 Martin P.J., Netterfield R.P., Kinder T.J. & Stanboul V. 1991, Ap.Phys.Lett., 58: 22, 2497  
 Martin S., Rivory J. & Schoenauer M. , 1995, Appl.Opt., 34, 2247  
 Noxon J.F., 1978, Planet.Space.Sci., 26, 191  
 Oliva E. & Origla L., 1992, A&A, 254 466  
 Osterbrock D.E., Fulbright J.P., Bida T.A., 1997, PASP, 109, 614  
 Piché F., 1996, Private Communication  
 Piché F., Parry I.R., Enrico K., Ellis R.S., Pritchard J., Mackay C.D. & McMahon R.G., 1997, in Ardeberd A., ed, Proc. SPIE 2871, Optical Telescopes of Today and Tomorrow: Following in the Direction of Tycho Brahe, 1332  
 Ramsay S.K., Mountain C.M. & Geballe T.R., 1992, MNRAS, 259, 751  
 Sobolev V.G., 1978, Planet.Space.Sci., 26, 703  
 Southwell W.H. 1985, Appl.Opt., 24, 456  
 Southwell W.H. & Hall R.L. 1989 Appl.Opt. 28 2949  
 Southwell W.H. 1989 Appl.Opt. 28 5091  
 Steed A.J. & Baker D.J., 1978, Appl.Opt., 18, 3386

## APPENDIX A: GENETIC ALGORITHMS

Genetic algorithms are optimisation techniques that draw on the Darwinian idea of evolution through survival of the fittest (Goldberg 1989). They are particularly suited to non-linear optimisation (minimisation or maximisation) problems with many distinct local minima where gradient following optimisation techniques will fail to find the global minimum. There are a number of possible implementations of the method. The method used here closely follows the algorithm described by Charbonneau (1995).

The basic steps are as follows:

- (i) Form a random initial population of solutions
- (ii) Assign a fitness value to each member of the population related to how closely it approached some desired solution
- (iii) Choose pairs of individuals from the population and form ‘offspring’ by breeding the two individuals. Introduce mutations into the genes.
- (iv) Establish the fitness of the offspring and, if they are fitter than the weakest member, insert them into the population
- (v) Repeat 2–4 until convergence is reached

An initial population of  $N_p$  individuals is created randomly. In the present case each member of the population

corresponds to a complete set of filter parameters,  $\delta_i, \alpha_i, \phi_i$  for  $i = 1, m$  where  $m$  is the number of sinusoids in equation 2. These *phenotypes* are decoded versions of their associated *genotypes*, the set of ‘genes’ that determine the parameters. Each individual has associated with it  $3m$  genes, each gene being a sequence of 5 integers between 0 and 9. The associated parameters are then given by interpreting the 5 integers as the first five significant figures of a real number between 0.0 and 0.99999. The parameters are then given by:

$$\delta_i = \delta_{max} \times x_{3i-2} \quad (i=1,2,3,\dots,m) \quad (A1)$$

$$\alpha_i = (\alpha_{max} - \alpha_{min}) \times x_{3i-1} + \alpha_{min} \quad (i=1,2,3,\dots,m) \quad (A2)$$

$$\phi_i = 2\pi \times x_{3i} \quad (i=1,2,3,\dots,m) \quad (A3)$$

where  $\alpha_{max}, \alpha_{min}$  and  $\delta_{max}$  are imposed constraints on the allowed range of the parameters. Here the  $x_k$  are given by:

$$x_k = \sum_{j=1}^5 10^{-j} I_{5(k-1)+j} \quad (A4)$$

where the  $I_j$  are the 5 integers representing the individual gene.

$$g_k = (I_{5k-4}, I_{5k-3}, I_{5k-2}, I_{5k-1}, I_{5k}) \quad (k=1,3m) \quad (A5)$$

The  $x_k$  serve to translate between the  $5 \times 3m$  integers representing the genotype, and the physical properties  $\delta_i, \alpha_i$  and  $\phi_i$ .

The population is ranked in order of fitness, however fitness is defined. In the present case the fitness is defined either as being related to the least squares deviation between the filter transmittance profile (Equation 4) or as an explicit function of the improvement in signal:noise ratio (Eq. 5).

Once the population is established, breeding can begin. Individuals are chosen for breeding with a probability proportional to their fitness ranking (Charbonneau 1995). When a pair of individuals are chosen the breeding operation is initialised by making copies of the parents. For example:

$$\text{Parent 1} = (I_1, I_2, I_3, \dots, I_{5 \times 3m}) \quad (A6)$$

$$\text{Parent 2} = (J_1, J_2, J_3, \dots, J_{5 \times 3m}) \quad (A7)$$

On breeding, and exchange of genes takes place. A random number is generated between 0 and 1. If this is less than a preset ‘cross-over’ probability then a random point is selected in the two genotype arrays of  $5 \times 3m$  integers, say position  $n$ . From that point forward the genes of the two parents are crossed to create two new individuals:

$$\text{Offspring 1} = (I_1, I_2, I_3, \dots, I_{n-1}, J_n, J_{n+1}, \dots, J_{5 \times 3m}) \quad (A8)$$

$$\text{Offspring 2} = (J_1, J_2, J_3, \dots, J_{n-1}, I_n, I_{n+1}, \dots, I_{5 \times 3m}) \quad (A9)$$

Mutation may also occur during breeding. A random number is selected for each of the  $5 \times 3m$  integers, if this is less than the (small) mutation probability the integer is replaced by a randomly chosen digit.

The genotypes of the two offspring are translated back into two sets of filter parameters and the fitness of the individuals is calculated. The population replacement strategy used is the ‘replace worst’ strategy described by Charbonneau (1995). If the fitness of the new individuals was greater than the weakest members of the population the weakest are

replaced by the new individuals. A generation is defined as a series of  $N_p$  breeding operations.

The rate of convergence of the solutions is rapid initially but becomes slow as the optimal solution is approached. The rate of convergence can be controlled to some extent by varying the mutation rate but other more direct optimisation techniques may be necessary to fine tune the solutions.